Nanoparticle-mediated targeting of MAPK signaling predisposes tumor to chemotherapy

Sudipta Basu[a,1], Rania Harfouche[a,1], Shivani Soni[a], Geetanjali Chimote[a], Raghunath A. Mashelkar[a,b,2], and Shiladitya Sengupta[a,2]

[a]Harvard-MIT Division of Health Sciences and Technology, Department of Medicine, Brigham and Women's Hospital, Harvard Medical School, Boston, MA 02115; and [b]National Chemical Laboratories, Pune 411008, India

Contributed by Raghunath A. Mashelkar, March 19, 2009 (sent for review December 4, 2008)

The MAPK signal transduction cascade is dysregulated in a majority of human tumors. Here we report that a nanoparticle-mediated targeting of this pathway can optimize cancer chemotherapy. We engineered nanoparticles from a unique hexadentate-polyD,L-lactic acid-co-glycolic acid polymer chemically conjugated to PD98059, a selective MAPK inhibitor. The nanoparticles are taken up by cancer cells through endocytosis and demonstrate sustained release of the active agent, resulting in the inhibition of phosphorylation of downstream extracellular signal regulated kinase. We demonstrate that nanoparticle-mediated targeting of MAPK inhibits the proliferation of melanoma and lung carcinoma cells and induces apoptosis in vitro. Administration of the PD98059-nanoparticles in melanoma-bearing mice inhibits tumor growth and enhances the antitumor efficacy of cisplatin chemotherapy. Our study shows the nanoparticle-mediated delivery of signal transduction inhibitors can emerge as a unique paradigm in cancer chemotherapy.

cancer | signal transduction

Cancer is the second leading cause of mortality in the United States, with an estimated 1,444,180 new cases and 565,650 deaths in 2008 (1). Standard chemotherapy nonspecifically targets all dividing cells, resulting in dose-limiting toxicities. Consequently, there is an urgent need to develop novel strategies that are more specifically targeted against the tumor. The MAPK pathway comprising of RAS, RAF, MEK, and ERK has been implicated in a majority of human tumors, often through gain of function mutations in the RAS and RAF families (2, 3). Indeed, RAS mutations occur in 30% of all cancer, and are particularly implicated in over 90% of pancreatic cancers (4) and 50% of colon cancers (5); RAF mutations are prevalent in over 60% of melanomas (6) and over 35% of ovarian cancers (7). As a result, the MAPK pathway has evolved as a focus of intense investigation for developing small molecule inhibitors as targeted therapeutics.

Another emerging strategy for targeted chemotherapy is to harness nanovectors for preferential delivery of drugs into the tumor (8). A wide range of nanovectors, including liposomes, micelles, polymeric nanoparticles, silicon and gold nanoshells, polymeric dendrimers, and carbon-based nanostructures, have been used for drug delivery to the tumor (9). It is well established that nanoparticles preferentially localize at the tumors as a result of the enhanced permeation and retention effect (10, 11). Indeed, a nanoliposomal formulation of cisplatin was shown to attain 10- to 200-fold increased drug concentration in tumors during a Phase-I clinical trial (12). However, standard liposomal or protein carrier-based nanoplatforms have limited control over drug release. In contrast, controlled-release drug delivery systems have the potential to induce standardized and durable clinical responses.

Interestingly, while extensive studies have been done on delivering cytotoxic agents to solid tumors using nanovectors, no report exists on combining targeted therapeutics with nanoparticle-based tumor targeting. In this study, we chemically conjugated a selective pharmacological inhibitor with a biodegradable polymer and engineered a nanoparticle that perturbs the MAPK signaling pathway. The nanoparticles enable sustained drug release, which results in inhibition of phosphorylation of ERK, a downstream signal in the MAPK signal-transduction cascade. This translates into inhibition of cancer cell proliferation and induction of apoptosis. Furthermore, we demonstrate that a nanoparticle-enabled targeting of the MAPK pathway inhibits tumor growth in vivo and enhances the anticancer activity of cisplatin, a first-line drug for the treatment of most cancers. Our results open up the possibility of harnessing nanovectors for modulating oncogenic pathways.

Results and Discussion

Synthesis and Characterization of Polylactic Acid Glycolic Acid-PD98059 Conjugates. Nanoparticles engineered from biodegradable, biocompatible, and Food and Drug Administration-approved polymers offer the potential for rapid translation to the clinics. As a result, we adapted polylactic acid glycolic acid (PLGA) as the starting polymer to engineer the nanoparticles. We selected PD98059 as the selective inhibitor to block MAPK signaling (13). To avoid the characteristic burst release associated with nanoparticles and achieve a controlled release profile, PD98059 was conjugated to linear PLGA 5050 **1**, using amide-coupling reaction to obtain PLGA-PD98059 (1:1) conjugate **2** (Fig. 1*A*). The loading of PD98059 in this conjugate was determined to be 3.0 μg/mg of polymer. To increase the drug loading, we modified the native PLGA **1** to generate hexa-carboxylic PLGA **8** using the scheme outlined in Fig. 1. The hexa-carboxylic PLGA **8** enabled conjugation of 6 molecules of PD98059 **9**, which increased the loading to 60 μg/mg (see Fig. 1*B*). The structure of molecules generated at each step was confirmed using spectroscopic and analytical methods [see supporting information (SI) *Materials and Methods*]. We used an emulsion-solvent evaporation method to formulate the nanoparticles from the conjugate **9** [PLGA-6(PD98059)] (14), which resulted in the formation of spherical nanoparicles with a median size distribution of 100 nm, as confirmed by transmission electron microscopy (TEM) and dynamic laser light scatter (DLS) (see Fig. 1*C*).

Engineering PEG Functionalized PD98059-Loaded Nanoparticles. Naked nanoparticles are rapidly cleared by the macrophages following opsonization. Surface modification of the nanoparticle with PEG has been reported to decrease surface interactions

Author contributions: S.B., R.H., S. Soni, G.C., R.A.M., and S. Sengupta designed research; S.B., R.H., S. Soni, and G.C. performed research; S.B. contributed new reagents/analytic tools; S.B., R.H., S. Soni, G.C., and S. Sengupta analyzed data; and S.B., R.H., S. Soni, R.A.M., and S. Sengupta wrote the paper.

The authors declare no conflict of interest.

[1]S.B. and R.H. contributed equally to this work.

[2]To whom correspondence may be addressed. E-mail: ram@ncl.res.in or shiladit@mit.edu.

This article contains supporting information online at www.pnas.org/cgi/content/full/0902857106/DCSupplemental.

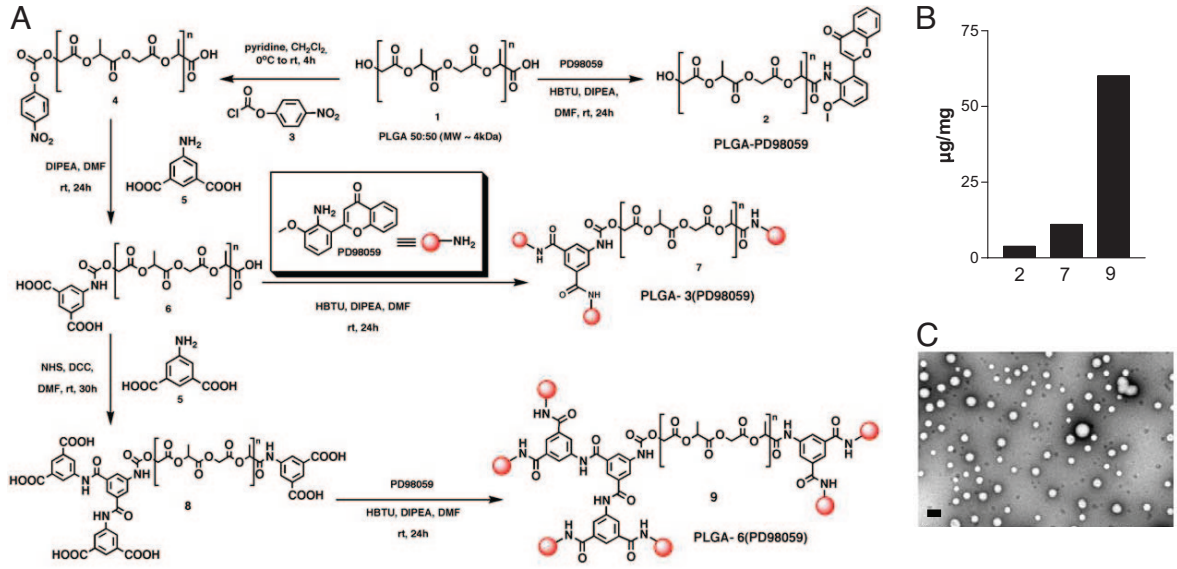

Fig. 1. Development of PD98059 loaded nanoparticles. (*A*) Synthetic scheme for different PLGA-(PD98059)$_x$ conjugates. (*B*) Loading of PD98059 in mono (*2*)-, tri (*7*)- and hexa (*9*)- dentate PLGA expressed as microgram per milligram of polymer. (*C*) Representative transmission electron microscopy image of nanoparticles synthesized from hexadentate PLGA-(PD98059)$_6$ conjugate. (Scale bar, 100 nm.)

with opsonins through steric repulsion (15), thereby conferring long-circulating property to the nanoparticles (16). PEG has excellent biocompatibility and is already approved by the Food and Drug Administration for human use (17). To develop the "stealth" nanoparticles (i.e., to mask them from tissue macrophages or the reticuloendothelial system), we synthesized a PLGA-*b*-PEG block copolymer **10** by amide coupling of the carboxylic acid of PLGA with the amine group of 2 KDa amine ethylene glycol using the coupling reagent HBTU with diisopropylethyl amine (DIPEA) as base (Fig. 2*A*). To optimize the size and surface coverage of the nanoparticles by PEG we used varying ratios of PLGA-*b*-PEG: PLGA-6(PD98059). Light scatter and TEM revealed that the PLGA-*b*-PEG: PLGA-6(PD98059) in 1:5 ratio gave the most optimal size distribution for further studies (see Fig. 2*A*).

To test whether a ratio of 1:5 of PLGA-*b*-PEG: PLGA-6(PD98059) confers optimal surface coverage of the nanoparticles by PEG, we developed a method based on the well-validated streptavidin-biotin binding to visualize the PEG chains on the surface of the nanoparticles using TEM. Biotinylated nanoparticles were engineered from a 1:5 mixture of PLGA-*b*-PEG-biotin conjugate **11** (Fig. S1) and PLGA. The nanoparticles were then probed with streptavidin-gold nanoparticles (5 nm), cross-sectioned, stained with uranyl acetate, and visualized using TEM. As seen in Fig. S1, the complexation of the gold nanoparticles at the periphery of the cross-section of PLGA-PEG-nanoparticles clearly demonstrates that the PLGA-nanoparticle was surface coated with PEG. No such binding was observed with nanoparticles that were constructed with nonpegylated PLGA.

In Vitro-Release Kinetics of PD98059 from Nanoparticles. We next studied the controlled-release kinetics of PD98059 from the nanoparticles. To mimic the clinical situation, we incubated the nanoparticles with tumor-cell lysates, and dialyzed the released PD98059 against PBS buffer (pH = 7). We used 3 different cancer-cell lines for this study, the B16/F10 melanoma cells, the MDA-MB-231 breast-cancer cells, and Lewis lung carcinoma (LLC) cells. As shown in Fig. 2*B*, incubation with lysates of MDA-MB-231, B16/F10, and LLC cells resulted in a sustained release of PD98059 from the nanoparticles, with a faster release evident with the MDA-MB-231 cell lysate as compared with B16/F10 and LLC cells.

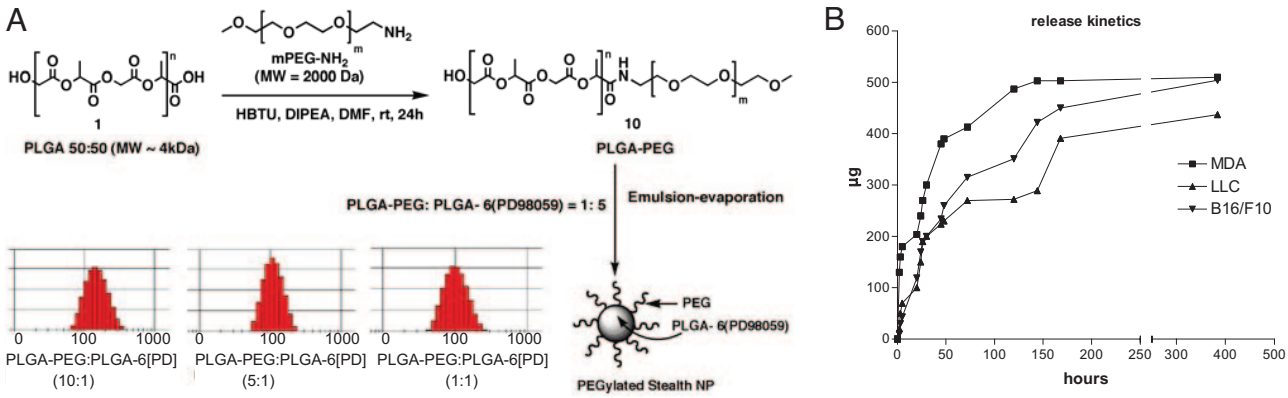

Fig. 2. Engineering pegylated nanoparticles. (*A*) Synthetic scheme for PEG-*b*-PLGA conjugate for engineering pegylated nanoparticles. Different ratio of PLGA-PEG: PLGA-[PD98059]$_6$ results in nanoparticles of different size distribution, as measured by DLS (*y*-axis = intensity; *x*-axis = size in nm). (*B*) Graph shows physicochemical release kinetics of PD98059 when the nanoparticles are incubated with MDA-MB231, LLC, and B16/F10 cell lysates.

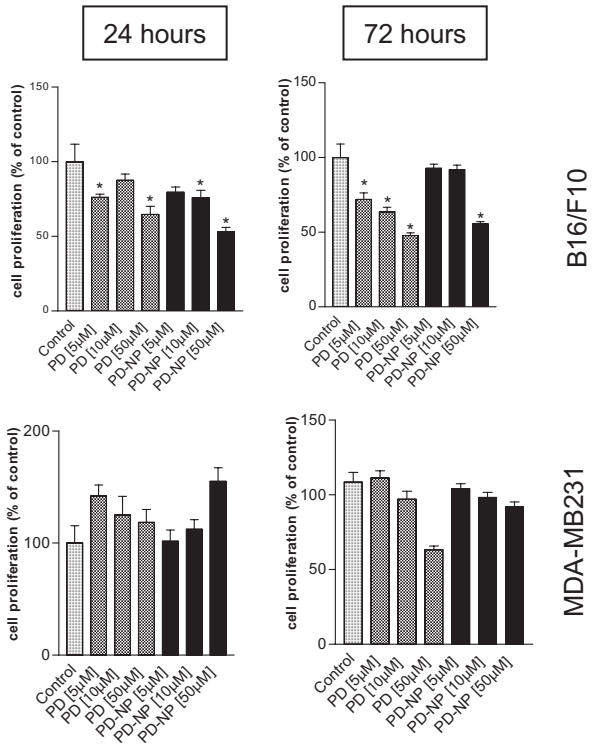

Fig. 3. Effect of PD98059-loaded nanopaticles on cell proliferation. B16/F10 melanoma and MDA-MB-231 breast-cancer cells were incubated with free PD98059 (PD), PD98059-nanoparticle (PD-NP), or vehicle (control), for 24 or 72 h. MTS assays were used to determine the temporal cytotoxicity of increasing concentrations of free PD98059 and PD98059-nanoparticles (NP). Data are expressed as percent of vehicle-treated control (considered as 100%), and represents mean ± SEM from at least triplicates. *, $P < 0.05$ vs. vehicle control (ANOVA followed by Dunnet's post hoc test).

In Vitro Cellular-Cytotoxicity Assay. We evaluated the anticancer effects of the PD98059-nanoparticle in a series of in vitro cytotoxicity assays. Western blot of the cell lysates confirmed the activated state of ERK, which is downstream of MEK signaling (data not shown), indicating that these were appropriate cells to study the effects of nanoparticle-mediated MAPK inhibition. Furthermore, to factor in the temporal-release kinetics of the nanoparticle, the cells were incubated for 24, 48, and 72 h in the presence of increasing concentrations of free drug or nanoparticles. The viability of the cells at the end of the incubation period was quantified using a colorimetric MTS assay. As shown in Fig. 3*A*, although there was more cytotoxicity at 24 h with the free drug as compared with the PD98059-nanoparticle treatment, this distinction was lost by 72 h, thus confirming the temporal-release control exerted by the nanoparticles. Interestingly, we observed different susceptibility to the PD98059-nanoparticle between cancer cell lines. After 72 h of incubation with nanoparticle (equivalent to 50-μM PD98059) treatment, the percentage of viable MDA-MB-231 cells (92%) was significantly greater than in the case of LLC (65%) (Fig. S2) or B16/F10 cells (55%), indicating that MDA-MB-231 is insensitive to the PD98059-nanoparticle. B16/F10 was found to be most susceptible, consistent with the up-regulated MAPK signaling in melanoma. In subsequent studies, we focused on the MDA-MB-231 and B16/F10 cell lines.

We evaluated apoptosis as a mechanism underlying the effect of treatment on cell viability. MDA-MB-231 and B16/F10 cells were treated with PD98059-nanoparticle (equivalent to 50-μM free PD98059) for 48 h, and then labeled with Annexin V-FITC, a marker for apoptosis. As seen in Fig. S3, PD98059-nanoparticle failed to induce significant apoptosis in MDA-MB-231 cells. In contrast, in the B16/F10 cell line, the free drug and PD98059-nanoparticle resulted in a 61-fold and a 360-fold increase in the number of cells in late apoptosis, respectively. This discrepancy between PD98059 and PD98059-nanoparticle is accounted for by the fact that the number of cells that were in the necrotic stage following free drug treatment was 51-fold higher than the cells treated with PD98059-nanoparticle, consistent with the sustained release of the active agent from the nanoparticle. We next evaluated the effect of the treatments on the phosphorylation status of ERK in MDA-MB-231 and B16/F10 cells. In the case of MDA-MB-231, the free drug inhibited ERK signaling by 5-fold, while the PD98059-nanoparticle had no significant effect. In contrast, both the PD98059 and PD98059-nanoparticles completely abolished the phospho-ERK signal in the B16/F10 cells (Fig. S4*A*). The differences in the phosphorylation of ERK may possibly explain the distinct outcomes in terms of cell viability for the 2 cell lines.

Internalization of Nanoparticles. To track the uptake and distribution of the nanoparticles in the cells, we engineered the nanoparticles from PLGA that was labeled with FITC. The temporal uptake of FITC-nanoparticle into the B16/F10 and MDA-MB231 cells was monitored over a 24-h period. The endosomal/lysosomal compartments in live cells were stained with the LysoTracker (*red*) probe. Merged images (*yellow*) following epifluorescence microscopy revealed that the FITC-nanoparticles were internalized into the lysosomes within 30 min in B16/F10, as seen by the colocalization of the signals. In contrast, internalization into MDA-MB-231 cells was slower than in the case of B16/F10 cells, and colocalization within endosomes/lysosomes was evident only at 12-h postincubation (Fig. S4*B*).

In Vivo Efficacy in B16/F10 Melanoma Model. To validate the antitumor efficacy of MAPK inhibition, we randomly sorted B16/F10 melanoma-bearing mice into 6 treatment groups: (*i*) vehicle control, (*ii*) free PD98059 (5 mg/kg), (*iii*) PD98059-nanoparticle (equivalent to 5 mg/kg of PD98059), (*iv*) cisplatin (1.25 mg/kg), (*v*) PD98059 (5 mg/kg) + cisplatin (1.25 mg/kg), and (*vi*) PD98059-nanoparticle (equivalent to 5 mg/kg of PD98059) + cisplatin (1.25 mg/kg). Cisplatin was administered i.p. 1 day after the PD98059 administration to achieve a sequential biological effect of MAPK inhibition, followed by induction of chemotherapy-induced cytotoxicity. The mice injected with the vehicle formed large tumors by day 14 and were killed. The animals in the other groups were also killed at the same time point to evaluate the effect of the treatments on tumor pathology.

As shown in Fig. 4*A*, the treatments resulted in significant tumor inhibition as compared to the vehicle-treated group. Interestingly, the combination of MAPK inhibition and the cytotoxic agent, cisplatin, exerted an enhanced antitumor outcome as compared to either drug alone. This is consistent with earlier reports, where MAPK inhibitors were found to synergize with cytotoxic agents (18). Indeed, gross pathological analysis of the tumor sections stained with H&E (Fig. 4*C*) revealed large necrotic areas following treatment with the PD98059-nanoparticles, cisplatin, and a significant increase when the 2 treatments were combined together. Interestingly, while the distinction between the mean tumor volume in the free PD98059 plus cisplatin and the PD98059-nanoparticle plus cisplatin-treated groups was statistically not significant, 50% of the animals in the latter group showed complete tumor ablation, as compared to none in the former. Although there was a statistically significant decrease in the body weight of animals following treatment (Fig. 4*B*), the total loss was less than 10%, which is the predicted cut-off value for indicating nonspecific toxicity (19).

To dissect the mechanism of action for the antitumor activity of the PD98059-nanoparticle and the synergism observed with

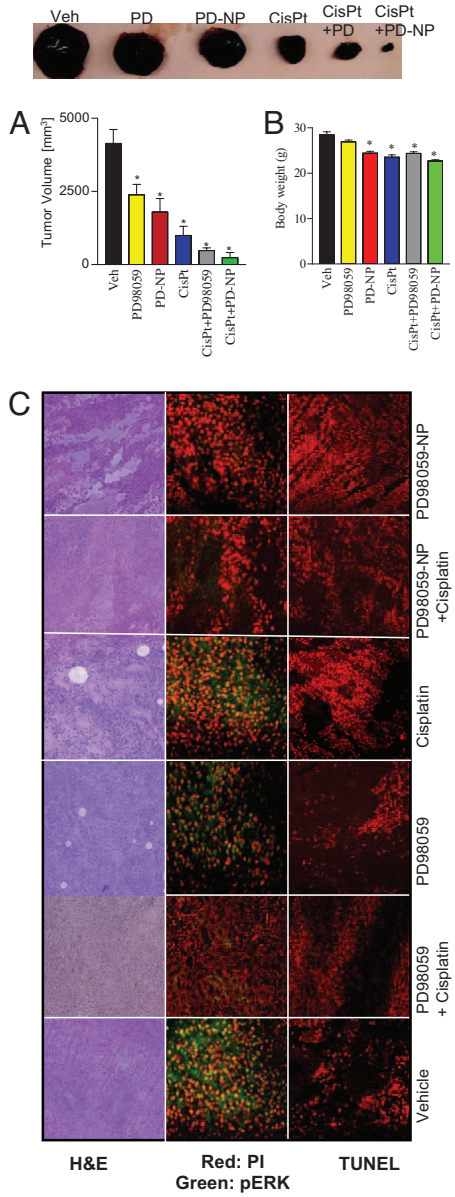

Fig. 4. Combination therapy of PD98059-NP with cisplatin inhibits B16/F10 melanoma in xenograft mouse model. (*A*) Graph shows tumor volume of B16/F10 melanoma in different treatment groups, comparing the effects of PD98059-nanoparticle (PD-NP) + cisplatin, PD-NP, free PD98059, cisplatin, and free PD90859 + cisplatin. The control group received saline. Animals were treated with PD98059 (free or NP-conjugated) at a dose of 5 mg/kg through the tail vein. Cisplatin (1.25 mg/kg) was administered i.p. 1 day after the PD98059 dosing. Animals were killed on day 14. Each animal received 3 doses of the treatments. (*B*) Mean body weight of animals in different treatments as a measure of gross toxicity. All results are mean ± SEM ($n = 6–8$ per treatment group). *, $P < 0.05$ vs. vehicle (ANOVA followed by Newman Keul's post hoc test). (*C*) Representative images showing histological staining of the cross section of the excised tumors in different treatments at 20× magnifications. (*Left*) H&E staining of representative tumor cross-sections. (*Middle*) Tumor cross-section was immunostained for phospho-ERK (*green*), and counter-stained with propidium iodide (*red*). (*Right*) Tumor sections were TUNEL-labeled for apoptosis with the use of Texas Red-labeled nucleotide. Images were captured using a Nikon Eclipse epifluorescence microscope.

cisplatin, we immunostained tumor cross-sections for phosphorylated ERK, which is downstream of the PD98059 target, MEK. As shown in Fig. 4*C*, treatment with PD98059 inhibited the intratumoral levels of phosphorylated ERK, as compared with vehicle-, free PD98059-, or cisplatin-treated groups. We next evaluated the tumors for apoptosis using TUNEL-staining. As shown in Fig. 4*C*, treatment with PD98059-nanoparticle and cisplatin induced significant levels of apoptosis, as compared with vehicle- or PD98059-treated tumors. Furthermore, the apoptosis induced by cisplatin was potentiated by the pretreatment with PD98059-nanoparticle, which could explain the greater antitumor outcome seen as compared with either drug alone.

Conclusion

MEK1/2 are dual-specificity kinases that phosphorylate and activate ERK, the classical MAP kinase (2). These kinases lie downstream of RAS/RAF, which are the most commonly mutated members of the MAPK pathway. Additionally, MEK/ERK signaling is also activated downstream of growth-factor tyrosine-kinase receptors, such as epidermal growth factor receptor and MET receptor, which are implicated in tumorigenesis (20, 21). As a result, targeting MEK or ERK offers the possibility of exerting an antitumor effect, even in the absence of RAS/RAF mutations. Activated ERK regulates the functions of multiple molecules that are implicated in the cell cycle, including $p21^{Cip1}$, $p16^{Ink4a}$, and $p15^{Ink4b}$. Furthermore, it can phosphorylate and inactivate proapoptotic Bad, resulting in activation of the antiapoptotic Bcl-2 (22). The inhibition of cell proliferation and the induction of apoptosis following treatment with free PD98059 or PD98059-nanoparticle are consistent with the inhibition of phosphorylation of ERK, and the resultant blockage of these downstream proliferative and antiapoptotic signals. Interestingly, while incubation with cell lysates from all of the 3 cell lines resulted in the release of the active agent from the nanoparticle at similar rates, only B16/F10 melanoma and LLC cells were susceptible to the PD98059-nanoparticles, and there was limited effect on the MDA-MB-231 breast-cancer cells. Our results suggest that this could arise from the variability in the uptake of nanoparticles into distinct tumor cells, indicating that intracellular uptake and processing is a critical factor in governing the susceptibility of a cancer cell to drug-conjugated nanoparticles. Further optimization of the nanoparticles with internalizing peptides or antibodies will be required for targeting cancer cells that exhibit limited internalization of nanoparticles. The display of biotin on the surface of the PEG-PLGA:PLGA-PD98059 in our study indicates that the internalizing peptides can be conjugated in a similar manner to the PEG chains. For example, Ruoslahti et al. (23) have demonstrated that an iRGD peptide cannot only target tumors in vivo but is also internalized, and can be used for active targeting of nanoparticles to tumors.

Interestingly, while free PD98059 exerted a superior effect in vitro as compared with the PD98059-nanoparticle at early time points, we observed a significant improvement in the therapeutic efficacy in vivo with the latter. Indeed, the group that recieved cisplatin plus PD98059-nanoparticles exhibited complete tumor ablation in some of the animals. This is consistent with earlier findings where a nanoparticle-conjugated drug had greater activity in vivo, and arises from the preferential delivery of the nanoparticles to the tumor and the sustained release of the drug (24). In a previous study, we observed an increased uptake of fluorescently labeled pegylated nanoparticles in the tumor in vivo (14). This is further validated by the greater inhibition of intratumoral ERK signaling and resulting apoptosis when treated with the PD98059-nanoparticles as compared with the free drug. Excitingly, this mechanism-based induction of apoptosis translated into a synergistic effect when combined with a traditional chemotherapeutic agent, cisplatin, which induces apoptosis by intercalating with the DNA.

Several components of the present study can facilitate future therapy in humans: (*i*) optimization of drug loading using the hexadentate PLGA can allow the achievement of clinically-

relevant doses; (*ii*) the increased in vivo efficacy of nanoparticle-MEK inhibitor as compared to the free drug indicates that nanoparticles could evolve as a powerful platform for targeting oncogenic pathways, while avoiding the off-target mechanism-driven effects of the inhibitors; and (*iii*) the synergistic effects observed when PD98059-nanoparticles were combined with cisplatin indicate that this could evolve as a powerful multi-pronged strategy for the management of cancer. In summary, this study describes a nanotechnology-based strategy for targeting cancer and when combined with cytotoxics may emerge as a previously unrecorded paradigm in the management of cancer.

Materials and Methods

Nanoparticle Synthesis and Characterization. Modified hexadentate PLGA was synthesized as described in the *SI Materials and Methods*. A 1:5 mixture of PLGA-PD98059 and PLGA-PEG conjugates were dissolved in acetone methanol. The entire solution was emulsified in 2% aqueous solution of PVA (80% hydrolyzed, Mw≈9,000–10,000) by slow injection with constant homogenization using a tissue homogenizer. This mini-emulsion was added to a 0.2% aqueous solution of PVA (80% hydrolyzed, Mw ≈9,000–10,000) with rapid mixing for 4 h at room temperature to evaporate any residual acetone or methanol. Nanoparticles were recovered by ultracentrifugation at 80,000 × *g*. Sizing and morphological analysis was performed by dynamic light scattering (Malvern Nanozetasizer) and TEM. Level of pegylation was determined using a gold-nanoparticle streptavidin biotin-based assay as described in the *SI Materials and Methods*. Release kinetics of active drug release was quantified using UV-VIS spectroscopy as described in the *SI Materials and Methods*.

Cell Viability Assay. Cancer cells in 96-well plates were incubated with increasing concentrations of the PD98059 or PD98059-nanoparticle for 24, 48, or 72 h. The percentage of viable cells was then quantified with MTS (CellTiter 96 AQueous One Solution) assay.

Apoptosis Study. Induction of apoptosis following treatment was quantified using AnnexinV-Alexa Fluor 488 binding. Cells were stained according to the manufacturer's protocol. Cells were counterstained with propidium iodide and immediately analyzed using a Becton Dickinson FACSCalibur flow cytometer.

Drug Uptake and Metabolism. MDA-MB-231 and B16/F10 cells were treated with FITC-conjugated nanoparticles for a time-course ranging from 30 min to 24 h. The endosomes/lysosomes were labeled with LysoTracker Red. Images were captured using an epifluorescence microscope (Nikon Eclipse).

Immunoblotting of Cell Extracts. Proteins were electrophoretically resolved on SDS/PAGE gel, transferred onto polyvinylidene difluoride membranes, blocked for 1 h with 7% nonfat dry milk, and subsequently incubated overnight at 4 °C with primary antibodies directed against the phosphorylated or total forms of ERK1//2 and AKT. Proteins were detected with HRP-conjugated anti-rabbit secondary antibodies and Lumi-LightPLUS Western blotting substrate. The blots were developed using GeneSnap, and optical density of the protein bands was quantified using GeneTools.

In Vivo Murine B16/F10 Melanoma Tumor Model. Male C57/BL6 mice (20 g) were injected with 5×10^5 BL6/F10 melanoma cells into the flanks. The drug therapy was started after the tumors attained a volume of 25 mm^3. The animals were injected through the tail vein with free PD98059 or PD98059-nanoparticles (equivalent dose of free PD98059, 5 mg/kg). Animals receiving cisplatin were injected with the cytotoxic (1.25 mg/kg, i.p.) after one day of the PD98059 administration. Tumor volume was measured as a function of the length and breadth using the equation $l \times b^2$. All animal procedures were approved by Harvard University Institutional Use and Care of Animals Committee.

Tumor Immunohistology. Permeabilized paraformaldehyde-fixed tumor sections from different treatment groups were probed for phospho-ERK and TUNEL (apoptosis) as described in the *SI Materials and Methods*, using a rabbit polyclonal primary antibody against phosphoERK (dilution 1:250).

Statistical Analysis: All results were expressed as mean ± SEM of at least triplicate samples. Statistical comparisons were obtained using 1-way analysis of variance. Probability (*P*) values less than 0.05 were considered significant.

ACKNOWLEDGMENTS. This study is supported by Department of Defense Breast Cancer Research Program Era of Hope Award W81XWH-07–1-0482, a Mary Kay Ash Charitable Trust Grant Award, and a Coulter Foundation Career Award (to S. Sengupta). R.H. is supported by a Canadian Institutes of Health Research Postdoctoral Fellowship.

1. Anonymous (2008) American Cancer Society. Cancer Facts and Figures 2008. Atlanta: American Cancer Society 2008. www.cancer.org/downloads/STT/2008CAFFfinalsecured.pdf
2. Downward J (2003) Targeting RAS signaling pathways in cancer chemotherapy. *Nat Rev Cancer* 3:11–22.
3. Davies H, et al. (2002) Mutations of the BRAF gene in human cancer. *Nature* 417:949–954.
4. Friday BB, Adjei AA (2008) Advances in targeting the Ras/Raf/MEK/Erk mitogen activated protein kinase cascade with MEK inhibitors for cancer therapy. *Clin Cancer Res* 14:342–346.
5. Bos JL, et al. (1987) Prevalence of ras gene mutation in human colorectal cancers. *Nature* 327:293–297.
6. Brose MS, et al. (2002) BRAF and RAS mutations in human lung cancer and melanoma. *Cancer Res* 62:6997–7000.
7. Sieben NL, et al. (2004) In ovarian neoplasms, BRAF but not KRAS mutations are restricted to low-grade serous tumors. *J Pathol* 202:336–340.
8. Peer D, et al. (2007) Nanocarriers as an emerging platform for cancer therapy. *Nature Nanotech* 2:751–760.
9. Zhang L, et al. (2008) Nanoparticles in medicine: therapeutic applications and developments. *Clin Pharmacol Ther* 83:761–769.
10. Allen TM, et al. (1991) Liposomes containing synthetic lipid derivatives of poly(ethylene glycol) show prolonged circulation half-lives in vivo. *Biochim Biophys Acta* 1066:29–36.
11. Yuan F, et al. (1994) Microvascular permeability and interstitial penetration of sterically stabilized (stealth) liposomes in a human tumor xenograft. *Cancer Res* 54:3352–3356.
12. Boulikas T, Stathopoulos GP, Volakakis N, Vougiouka M (2005) Systemic Lipoplatin infusion results in preferential tumor uptake in human studies. *Anticancer Res* 25:3031–3039.
13. Alessi DR, et al. (1995) PD098059 is a specific inhibitor of the activation of mitogen-activated protein kinase kinase in vitro and in vivo. *J Biol Chem* 270:27489–27494.
14. Sengupta S, et al. (2005) Temporal targeting of tumor cells and neovasculature with a nanoscale delivery system. *Nature* 436:568–572.
15. Mosqueira VC, et al. (2001) Relationship between complement activation, cellular uptake and surface physicochemical aspects of novel PEG-modified nanocapsules. *Biomaterials* 22:2967–2979.
16. Moghimi SM, Hunter CA, Murray CJ (2001) Long-circulating and target-specific nanoparticles: theory to practice. *Pharmacol Rev* 53:283–318.
17. Fishburn CS (2008) The pharmacology of PEGylation: balancing PD with PK to generate novel therapeutics. *J Pharm Sci* 97:4176–4183.
18. Cui W, et al. (2000) Cisplatin-induced response of c-jun N-terminal kinase 1 and extracellular signal–regulated protein kinases 1 and 2 in a series of cisplatin-resistant ovarian carcinoma cell lines. *Mol Carcinog* 29:219–228.
19. Clark DL, et al. (1999) Predictive value of preclinical toxicology studies or platinum anticancer drugs. *Clin Cancer Res* 5:1161–1167.
20. Marks JL, et al. (2008) Novel MEK1 mutation identified by mutational analysis of epidermal growth factor receptor signaling pathway genes in lung adenocarcinoma. *Cancer Res* 68:5524–5528.
21. Sengupta S, et al. (2003) Targeting of mitogen-activated protein kinases and phosphatidylinositol 3 kinase inhibits hepatocyte growth factor/scatter factor-induced angiogenesis. *Circulation* 107:2955–2961.
22. McCubrey JA, et al. (2007) Roles of the Raf/MEK/ERK pathway in cell growth, malignant transformation and drug resistance. *Biochemica et Biophysica Acta* 1773:1263–1284.
23. Ruoslahti E, Duza T, Zhang L (2005) Vascular homing peptides with cell-penetrating properties. *Curr Pharm Des* 11:3655–3660.
24. Tang N, et al. (2007) Improving penetration in tumors with nanoassemblies of phospholipids and doxorubicin. *J NatlCancer Inst* 99:1004–1015.